Long-term forcing of Sun's coronal field, open flux and cosmic ray modulation potential during grand minima, maxima and regular activity phases by the solar dynamo mechanism

Soumyaranjan Dash[1], Dibyendu Nandy[1,2]★, Ilya Usoskin[3]
[1]Center of Excellence in Space Sciences India, Indian Institute of Science Education and Research Kolkata, Mohanpur 741246, West Bengal, India
[2]Department of Physical Sciences, Indian Institute of Science Education and Research Kolkata, Mohanpur 741246, West Bengal, India
[3]Space Physics and Astronomy Research Unit and Sodankylä Geophysical Observatory, University of Oulu, Finland

26 August 2022

ABSTRACT

Magnetic fields generated in the Sun's interior by the solar dynamo mechanism drive solar activity over a range of time-scales. While space-based observations of the Sun's corona exist only for few decades, direct sunspot observations exist for few centuries, solar open flux and cosmic ray flux variations can be reconstructed through studies of cosmogenic isotopes over thousands of years. While such reconstructions indicate the presence of extreme solar activity fluctuations in the past, causal links between millennia scale dynamo activity, consequent coronal field, solar open flux and cosmic ray modulation remain elusive. By utilizing a stochastically forced solar dynamo model we perform long-term simulations to illuminate how the dynamo generated magnetic fields govern the structure of the solar corona and the state of the heliosphere – as indicated by variations in the open flux and cosmic ray modulation potential. We establish differences in the nature of the large-scale structuring of the solar corona during grand maximum, minimum, and regular solar activity phases and simulate how the open flux and cosmic ray modulation potential varies over time scales encompassing these different phases of solar activity. We demonstrate that the power spectrum of simulated and reconstructed solar open flux are consistent with each other. Our study provides the theoretical basis for interpreting long-term solar cycle variability based on reconstructions relying on cosmogenic isotopes and connects solar internal variations to the forcing of the state of the heliosphere.

Key words: Sun: activity – Sun: corona – Sun: evolution – Sun: heliosphere

1 INTRODUCTION

The variability of solar magnetic activity over long time scales is manifested in multiple observable proxies. Direct solar observations for the past ~ 400 years have revealed significant variability in the solar magnetic cycle, covering a period of extremely quiet Maunder minimum (second half of the 17th century) to a period of increased activity (middle of the 20th century). Modulations in solar cycle amplitude and duration are the indicators of such fluctuations. The impact of solar magnetic field dynamics on the state of the heliosphere as it emerge through the surface, evolve and extend into the solar corona is experienced via the open solar flux. It is the distribution of the coronal magnetic fields that provides us an idea of the solar open flux. Magnetic activity evolution of the Sun and other stars directly impact the environment of the harboured planets (Nandy 2004; Nandy & Martens 2007; Bharati Das et al. 2019). Our current understanding of the long-term solar variability and its impact on solar system planets with observations, reconstructions and theoretical modeling has improved over the years (Nandy et al. 2021). One of the critical questions which piqued the interest of the scientific community is whether grand minima and maxima episodes are the outcome of special states of the solar dynamo mechanism or if they result from random variability (Nandy et al. 2011; Choudhuri & Karak 2012; Carbonell et al. 1994). Our knowledge of the evolution of solar magnetic dynamo is limited by inadequate direct solar observations, which only exists from the early 17th century onwards, to definitively explain the reason behind such extreme episodes. Therefore, reconstructing its past history over longer periods is crucial. This is done by studying cosmogenic isotopes such as ^{10}Be (in polar ice cores) and ^{14}C (in tree rings) recorded in natural independently dated archives. Usoskin et al. (2003); Solanki et al. (2004); Usoskin (2017); Wu et al. (2018) have reconstructed the past solar activity over a multi-millennium time scale. Such reconstructions help us understand the solar activity level in the past and we can make deductions about solar magnetic activity driven terrestrial effects and space weather phenomena covering all possible activity ranges (e.g. Usoskin et al. 2007, 2015; Schröder 1992; Silverman 1992; Lockwood et al. 2017; Hayakawa et al. 2020; Isobe et al. 2019; Pal et al. 2020). But they lack description of the coronal magnetic field distribution which governs the space climate modulation.

Long-term solar dynamo simulations with stochastic fluctuations in the poloidal-field source can generate the extreme fluctuations with grand maximum and minimum like episodes (Passos et al. 2014; Tripathi et al. 2021; Albert et al. 2021). Magnetic field dynamics in the solar interior is manifested on the solar surface. The surface magnetic field evolution governs the solar coronal dynamics. It is the coronal

★ E-mail:dnandi@iiserkol.ac.in

magnetic field evolution that plays a key role in modulating galactic cosmic rays and our space environment. The distribution of the large-scale coronal magnetic fields which open into the heliosphere, facilitates the flow of solar wind plasma into the inter-planetary medium and impacts the propagation of cosmic ray particles. Due to lack of coronal magnetic field observations, we have a very limited understanding of its dynamics during past grand maxima and minima phases. Hence it is imperative to understand the large scale coronal magnetic field configuration. One of the measurable quantity in this regard is the open solar flux (OSF). Riley et al. (2015) modelled coronal magnetic field for solar minimum phase with global magnetohydrodynamic simulations. This gives us an idea about the coronal magnetic field configuration during a solar activity minimum. Lockwood & Owens (2021); Hayakawa et al. (2021, 2020) discussed about the configuration of the global solar corona during past eclipses recovered from historic paintings and observations. In this study we aim to understand the large-scale magnetic field configuration of the solar corona for fluctuating solar magnetic activity phases and subsequently study its impact on the state of the heliosphere. In order to map the solar coronal magnetic fields, we couple coronal magnetic field extrapolation models with solar dynamo simulations. One of the techniques to model the global solar coronal magnetic field, is the Potential Field Source Surface (PFSS) extrapolation (Altschuler & Newkirk 1969; Schatten et al. 1969; Schrijver & De Rosa 2003). In PFSS modeling technique, we assume the solar corona to be current free till the source surface (source surface is an imaginary surface within which coronal magnetic field is assumed to be current free and beyond the source surface the magnetic field is purely radial in nature) and reconstruct the magnetic fields utilizing the photospheric magnetic field as a boundary condition. PFSS models do not capture the non-potential nature of the active region coronal magnetic fields. However, the large-scale global coronal configuration is reasonably captured by the PFSS extrapolation technique. Predictive techniques with coupled surface flux transport model and the PFSS extrapolation provide reasonably accurate coronal magnetic field configurations (Nandy et al. 2018; Dash et al. 2020). The large scale coronal structure does not vary significantly over short time scales.

Modulations in the solar open flux and the cosmic ray modulation potential describe the impact of solar activity variation on heliospheric and cosmic-ray variability. Usoskin et al. (2021) reconstructed the OSF for past ~1000 years utilizing the cosmic ray flux assessed from cosmogenic-isotope ^{14}C measurements in tree rings (Brehm et al. 2021). A study by Lockwood & Owens (2014) shows reconstructed OSF using in-situ magnetic field observations for the last decade. From these reconstructions, we observe the OSF variation which is a result of spatially integrated coronal magnetic fields. The spatial distribution of the coronal magnetic fields which shows the large-scale structuring of the solar corona can not be recovered with these reconstructions.

In this study we explore the coronal magnetic field configuration during regular activity, grand maximum and grand minimum phases. We also explore the causal connection between the reconstructed solar activity and the special states of the solar dynamo by coupling the solar dynamo simulations to a PFSS model. We calculate the cosmic-ray modulation potential using the computed open solar flux from potential coronal magnetic field distribution. Numerical model setups are explained in Section 2. We present our results explaining the variations in magnetic field strength, coronal magnetic field configuration, OSF and cosmic ray modulation potential for different solar activity episodes in Section 3. Finally we conclude with discussions where we establish causality between the solar dynamo and past solar activity reconstructions. We demonstrate that our simulation results are consistent with the power spectrum of reconstructed open solar flux time series and discuss intriguing trends we find in the simulation and reconstructed data.

2 THEORETICAL MODELING

2.1 Solar Dynamo model

We solve the Babcock-Leighton (BL) dynamo model with imposed stochastic fluctuations on the alpha source. The model solves the following dynamo equations (1) and (2) in the kinematic regime in two dimensions using the `Surya - code` (Nandy & Choudhuri 2001, 2002; Chatterjee et al. 2004). The time evolution of the axisymmetric vector potential (A(r, θ)) for poloidal component and axisymmetric toroidal component (B(r, θ)) of the magnetic field are given by the following equations,

$$\frac{\partial A}{\partial t} + \frac{1}{s}\left[\mathbf{v_p}\cdot\nabla(sA)\right] = \eta_p\left(\nabla^2 - \frac{1}{s^2}\right)A + \alpha B \quad , \quad (1)$$

$$\frac{\partial B}{\partial t} + s\left[\mathbf{v_p}\cdot\nabla\left(\frac{B}{s}\right)\right] + (\nabla\cdot\mathbf{v_p})B = \eta_t\left(\nabla^2 - \frac{1}{s^2}\right)B + s(B\cdot\nabla\Omega) + \frac{1}{s}\frac{\partial(sB)}{\partial r}\frac{\partial\eta_t}{\partial r} \quad , \quad (2)$$

where, $s = r\sin(\theta)$. The poleward transport velocity which advects and distorts the magnetic field in each hemisphere by a single cell meridional flow is represented by $\mathbf{v_p}$ and Ω denotes the differential rotation in the solar convection zone (SCZ). In this model, we assume different magnetic diffusivities for the poloidal and toroidal field components, namely η_p and η_t respectively. In the numerical model, α is a source term that emulates the BL mechanism. This can be decomposed into two components, the mean field α-source (α_{MF}) – which operates in the bulk of the SCZ and the Babcock-Leighton α-source (α_{BL}) – that operates near the surface. Stochastic fluctuations are added to the source terms for both the hemispheres independently. Variations in the α_{BL} mimics the modulation in the surface BL mechanism towards magnetic bipoles of varied tilt angles whereas the α_{MF} dictates the level of turbulent convection of the flux tubes in the deep interior. The turbulent buffeting of the buoyant magnetic flux tubes rising through the SCZ adds a random component to the dispersion in the tilt angle distribution. The weak mean field alpha effect (α_{MF}) operates in the bulk SCZ on weak flux tubes which do not participate in formation of sunspots on the solar surface. Hence even during extremely low activity periods like solar minimum, α_{MF} remains operational. For simulating variable solar activity phases we employ BL dominated source term with proper quenching which is given by:

$$\alpha_{BL} = \alpha^0_{BL}\frac{\cos\theta}{4}\left[1+\mathrm{erf}\left(\frac{r-r_1}{d_1}\right)\right]\times\left[1-\mathrm{erf}\left(\frac{r-r_2}{d_2}\right)\right] \times a_1\left[1+\mathrm{erf}\left(\frac{B_\phi^2 - B_{1lo}^2}{d_3^2}\right)\right]\times\left[1-\mathrm{erf}\left(\frac{B_\phi^2 - B_{1up}^2}{d_4^2}\right)\right] \quad , \quad (3)$$

The detail description and the grounds of the quantities mentioned in equation (3) and their mathematical parameterisation, are available in Passos et al. (2014). We note that the quenching terms involving B_{1up}, B_{1lo} is incorporated into the expression for α_{BL}. These are important from a physical perspective because toroidal fields which are very weak cannot contribute to poloidal field generation, and very strong toroidal fields which are devoid of tilt again do not produce polar fields.

We use the stochastic nature of the poloidal source – traditionally the α effect (Choudhuri 1992; Charbonneau & Dikpati 2000; Proctor 2007; Brandenburg & Spiegel 2008; Moss et al. 2008), which generates fluctuations in the solar activity (Choudhuri 1992; Hoyng et al. 1994; Charbonneau et al. 2004; Usoskin 2008; Passos et al. 2014). The dispersion in the source term distribution controls the poloidal field amplitude and thus the solar cycle peak strength. Random stochastic fluctuations of strength 150% are introduced along with the mean value of the α_{BL}, denoted by α^0_{BL}, so that $\alpha_{BL} = \alpha^0_{BL}$ + α^{fluc}_{BL} σ(t,τ). Here, α^0_{BL} is set to 27 ms^{-1} and σ is the random values between [-1.5,1.5] picked after each coherence time τ (here 6 months). α^{fluc}_{BL} is set to the same value as α^0_{BL}. All other input parameters and flow profiles are adapted from Passos et al. (2014). We have computed the dynamo solutions for 6000 years.

Sunspot number is an important indicator of the solar cycle. In our study we use toroidal component of the magnetic field value as a proxy for the sunspot number. We identify the time and location where the value of B_ϕ exceeds a critical threshold $B_c = 8 \times 10^4$G as sunspot eruption proxies. If we count the number of such eruption episodes then we can model the sunspot proxy time series. This is a proxy of the sunspot number hence this should not be compared to the observed sunspot number time series quantitatively. We have also calculated the surface radial magnetic field using the magnetic vector potential A using the following expression:

$$B_r = \frac{1}{Rsin\theta}\left[\frac{\partial(Asin\theta)}{\partial\theta}\right] \quad . \tag{4}$$

In this paper we intend to understand the qualitative nature of the magnetic field evolution hence the simulation results are not suitable for direct comparison to the observed quantities.

2.2 Solar coronal magnetic field model

Reconstruction of large scale coronal magnetic fields can be done following Potential Field Source Surface extrapolation (PFSS) model (Schatten et al. 1969; Altschuler & Newkirk 1969) utilizing the surface radial magnetic field as boundary condition. This technique assumes the solar corona to be current free till the source surface (of radius $r = R_{ss}$). Beyond the source surface the impact of solar wind is dominant which makes the magnetic field lines purely radial. Hence in the region $R_\odot \leqslant r \leqslant R_{\rm ss}$,

$$\nabla \times \mathbf{B} \quad = \quad 0. \tag{5}$$

We can express the magnetic field in terms of a scalar field ϕ – which is the potential of the magnetic field – that satisfies,

$$-\nabla\phi \quad = \quad \mathbf{B}. \tag{6}$$

Since $\nabla \cdot \mathbf{B} = 0$ we can write,

$$\nabla^2\phi \quad = \quad 0. \tag{7}$$

By solving for the scalar potential (ϕ) we can compute the solar coronal magnetic fields within the source surface. Magnetic field observed on the solar surface is used as the boundary condition for extrapolation. We assume that near the source surface ($R_{ss} = 2.5R_\odot$), the magnetic field is purely radial. This coronal magnetic field modeling technique is widely used in the solar physics community to compute the large scale configuration of the corona. For detailed derivation of the model equations, refer to Schrijver & De Rosa (2003). We compute the coronal magnetic fields using the solar dynamo generated surface magnetic field (B_r) distribution as the lower boundary condition. We can derive the open solar flux near the source surface by integrating $|B_r|$ over the source surface (R_{ss} = 2.5 $R_\odot$).

2.3 Cosmic ray modulation potential

The process of the heliospheric cosmic-ray modulation is complex (Potgieter 2013) but is often parameterized via heliospheric parameters such as OSF or the modulation potential (e.g. Usoskin et al. 2002; Wu et al. 2018). The cosmic-ray modulation potential describes the mean deceleration (energy/rigidity loss) of galactic cosmic-ray particles within the heliosphere modulated by solar activity. Solar wind carries turbulent magnetic field ans solar wind plasma from the solar corona into the interplanetary medium. Solar forcing on the cosmic ray modulation (parameterized as cosmic ray modulation potential) is mediated via the open solar flux. We calculate cosmic ray modulation potential (Φ) using a semi-empirical formalism given by Asvestari & Usoskin (2016),

$$\Phi = \Phi_0 \times F^{n-\frac{\theta}{\theta_0}}(1 - \beta p). \tag{8}$$

Here Φ, F, θ denote the modulation potential, open solar flux and the heliospheric tilt angle respectively. The free parameters in eqn-8 Φ_0, θ_0, n and β are adopted from Asvestari & Usoskin (2016) as: Φ_0 = 1473.9 MV, θ_0 =150°, n =1.03 and β = 0.095. In equation-8, p denotes the polarity of the solar magnetic field. We assign the polarity p= +1 (positive)/ -1 (negative) depending on the polarity of the solar poles (for our calculations we consider solar north pole as reference) in our calculation. The solar open flux (F) is calculated at the source surface $R_{ss} = 2.5R_\odot$ and normalized with the maximum value. Normalized OSF is used to compute the modulation potential. In our 6000-year simulation the maximum value of the OSF is 1.817×10^24 Mx. The tilt angle (θ) denotes the average angle between the heliospheric current sheet and the equatorial plane. For our calculations, the tilt angle is the angle subtended by the line joining the Sun's center and the source surface neutral line (i.e. where $B_r = 0$) with respect to solar equator. We calculate cosmic-ray modulation potential for 6000-year dynamo run.

3 RESULTS

The stochastic forcing imposed on α_{BL} generates random occurrences of fluctuating solar activity (ranging from grand maxima to grand minima) cycles. In the top panel of Fig-1, we show the butterfly diagram of surface magnetic field (B_r) for 6000 years. Here the color red/blue denotes the positive/negative polarity. We also plot the latitudes of sunspot eruptions over the butterfly diagram (in black). OSF for the same temporal range with annual cadence is plotted in the middle panel which indicates the impact of solar activity variation on the state of the heliosphere. The magenta curve shows the time series of OSF. A 22 year moving average of the OSF in solid black curve is plotted to emphasize the long-term trends. In order to assess the impact of solar activity on cosmic ray flux we compute the cosmic ray modulation potential. The time series of cosmic ray modulation potential is shown in green solid line in the bottom panel of Fig-1. Similarly we plot the 22-year moving average of the cosmic ray modulation potential in solid black line over the green curve.

Solar activity variation can be broadly divided into two classes which are grand minima phase and regular phase (Tripathi et al. 2021). The regular phase covers grand maximum like enhanced magnetic activity and the regular activity phase. In order to identify different phases of solar activity periods we plot the solar dynamo model generated sunspot proxy time series (shown in Fig-2). Grand maxima episodes correspond to strong magnetic activity. We identify such periods with a threshold of mean sunspot number + 3σ (red dashed line in Fig-2). Episodes beyond this cut-off are defined

as grand maxima phases. During such phases, the sunspot eruptions are observed to appear till high latitudes in our simulation. Solar activity phases with no sunspot eruptions (at least for three consecutive cycles) are defined as grand minima phases. The green dashed line denotes global mean of the sunspot number proxy in the top panel of Fig-2). During regular activity phases the sunspot eruption proxy remains close to the global mean. In our simulation we find multiple instances of grand minima, maxima and regular activity phases. We notice a decrease in the OSF and cosmic ray modulation potential time series for grand minimum phases. In Fig-3 we discuss the coronal magnetic field configuration starting from a cycle minimum for three different phases of solar activity phases namely grand maxima (year 1967, 1971, 1975 and 1979), grand minima (year 2133, 2137, 2141 and 2145) and regular solar activity (year 2296, 2300, 2304 and 2308). The variation of magnetic field strength corresponding to these three phases is apparent in our simulation (see Fig-4). In order to further analyze these different phases in detail, we select a period from 1900 to 2500 years that encompasses all the three phases on the solar activity variation and demonstrate the coronal magnetic field configuration at cycle maximum and minimum (in Fig-5).

3.1 Solar corona during grand maxima, grand minima and a regular solar activity period

The evolution of the state of the heliosphere by the solar coronal magnetic fields can be parameterized by OSF which in turn impacts the cosmic ray modulation. OSF and the cosmic ray modulation potential are spatially averaged quantities. This implies they lack description of solar coronal magnetic field distribution. The nature of the solar coronal magnetic fields (whether they are open or closed within the solar source surface) significantly impact the flow of solar wind plasma in to the heliosphere.

Grand maxima phase corresponds to a period where the magnetic activity of the Sun is elevated than usual. We analyze one of such grand maxima phases which spans from year 1967 to 1979 in our simulation. In this phase, the sunspot proxies are observed near high latitudes (red shaded region in the bottom panel of Fig-3). For this grand maxima phase we plot the coronal magnetic field configuration starting from the cycle minimum at each 4 years. Open field lines are shown in blue (radially outward) and magenta (radially inward). The closed field lines are denoted by black curves. As the cycle progresses, numerous sunspot eruptions result in increasingly complex coronal magnetic field configuration. This is depicted by the top panel of Fig-3 corresponding to (a) Grand Maxima.

Grand minimum phase is identified as a period where there are no sunspot eruptions on the solar surface. We choose a time period from year 2133 to 2145 for our study which is shaded in yellow in the bottom panel of Fig-3. Coronal magnetic field configuration during grand minimum phase at each 4 years is provided in Fig-3 (Grand Minima). The magnetic field configuration during this phase shows complex closed loop structures. Although the magnetic field strength during grand minimum is less than regular and grand maximum phases, the complex structuring of solar corona leads to decrease in the solar forcing of the heliosphere via OSF.

We identify the phase from year 2269 to 2308 as regular solar activity phase. During this episode, the number of sunspot proxies lie between the grand maxima phase (red dashed curve in the top panel of Fig-2) and the global mean (green dashed curve in the top panel of Fig-2). For a regular phase the global coronal structure is not fundamentally different than that of a grand maxima phase. However, during this phase global parity of the Sun shifts from dipolar to quadrupolar in our simulation (change in the polar field can be confirmed by the change in open field line polarity in Fig-3 for the panel corresponding to regular solar activity). Similar parity change in Sun's magnetic field for a long-term solar dynamo simulation is reported by Hazra & Nandy (2019).

As the solar activity decreases, the strength of the magnetic field also varies. We calculate the integrated radial magnetic flux at different heights by computing $\int B_r(r,\theta) r d\theta$ for different solar activity phases to asses the magnetic field amplitude. Here r varies from r=R$\odot$ to r=2.5R$\odot$ in ten equal steps. At the source surface r=2.5R$\odot$, the calculated quantity shows the open solar flux. The variation of $\int B_r(r,\theta) r d\theta$ is calculated for grand maxima, grand minima and regular solar activity phase. In Fig4 (top) coronal magnetic field configuration is shown for these phases. The integrated flux of radial magneic field at different radial distances is plotted in Fig4 (top-right). For different phases – grand maximum (blue), regular solar activity (green) and grand minimum (red) phase – the magnetic field strength reduces gradually in correspondence with the solar activity level. Hence the strength of solar forcing on the state of the heliosphere varies accordingly which is reflected in the OSF and cosmic ray modulation potential (see Fig-1).

3.2 Solar corona during cycle maximum and minimum

In the sunspot butterfly diagram there are different cases of sunspot distribution based on their hemispheric appearance. In Fig-5 we demonstrate the coronal magnetic field configuration corresponding to solar cycle maximum (in the bottom panel) and minimum (in the top panel) for such cases. Cycle maxima and minima are chosen at a temporal difference of 7 years for all the cases in our study to maintain uniformity. Time-latitude distribution of surface radial field and the sunspot eruption proxies from solar dynamo simulation is shown in the middle panel with the sunspot eruption latitudes over-plotted in black. For year 1969, the sunspot eruption proxies are observed to extend till high latitudes. The corresponding coronal magnetic field configuration shows closed magnetic loops near the equatorial region. As we progress through this cycle (year 1977), we notice similar complexity in the coronal magnetic field distribution as well. We isolate a period where sunspot eruptions are absent in the northern hemisphere (year 2079). In the bottom panel, for cycle maximum we find a dipolar configuration of the solar corona with multiple closed loop structures. The year 2086 which indicates the cycle minimum, shows a change in parity of the solar corona. Such parity reversal in long term solar dynamo simulations is reported by Hazra & Nandy (2019) for phases where the sunspot eruption is decoupled across hemispheres. As we approach towards a grand minimum phase sunspot eruption proxies become zero. Year 2133 indicates such a case where there are no sunspot eruptions in both the hemispheres. In this phase, we find a complex coronal magnetic field (although the magnitude of the magnetic field is weak) configuration corresponding to both maximum and minimum of the solar cycle. When there are no sunspots eruptions in the southern hemisphere (year 2479), a quadrupolar parity of the solar magnetic field is observed. Distribution of coronal magnetic fields indicate presence of closed loops for this case. Even for the solar cycle maximum (year 2485) corresponding to this period solar corona retains the quadrupolar parity.

3.3 Suppressed 11-year cycle period during grand minimum episodes

Solar activity follows a dominant 11-year cycle period. Cyclic variability of this solar activity can be explored using spectral analysis.

In order to understand the periodicities present in the time series during a grand minimum episode we perform spectral analysis on the open solar flux and the cosmic ray modulation potential time series for grand minimum phases present in our 6000-year simulation. These phases are observed for year 998 to 1140 (142 years), year 2099 to 2245 (146 years), year 3995 to 4099 (104 years) and year 4904 to 5120 (216 years). During these grand minimum phases there were no sunspot-proxies found on the solar surface in our simulation (see Fig-1). We demonstrate the power spectrum of OSF and cosmic ray modulation potential on the longest grand minimum phase (year 4904 to 5120) in our simulation. We use fast Fourier transform (FFT) with an annual cadence for our analyses. OSF and modulation potential time series were normalized to the global maximum value of the respective time series which are 1.8170e+24 Mx and 1614 Mv respectively. Fig-6 and 7 shows the time series and the power spectrum for OSF and cosmic ray modulation potential respectively.

Regular activity phase corresponds to a period where we observe finite sunspot proxies (as opposed to zero sunspot-proxies during a grand minimum phase) on the solar surface (see Fig-1). The red curve in Fig-6(a) shows the normalized time series of OSF for one of the regular phase of equal length (216 years) as grand minimum phase. The regular phase covers OSF variation from year 432 to 648. In the panel Fig-6(b) the power spectrum is plotted. The brown dotted curve denotes 11 year cycle period for reference. For this case, Fourier power corresponding to the 11-year cycle is prominent as expected. The over all magnetic activity decreases during grand minimum which might lead to increased noise levels in the time series. Hence, we perform FFT analysis on randomly re-sampled data sets of OSF and cosmic ray modulation potential for 1000 times and compute the upper 95th percentile of the power spectrum which is defined as our confidence level (CL). We randomly shuffle each dataset (grand minimum and regular phase) for re-sampling. The confidence level (CL) is denoted by the black dashed curves in Fig-6(b) and 6(d).

Figure-6(c) denotes OSF variation during grand minimum phase. The corresponding power spectrum is shown in Fig-6(d). The dominant power is accumulated against 9.3 years period. It is important to note that the spectral power decreases significantly in the grand minimum phase as compared to the regular phase. There are few other periodicities which are present towards higher time periods. However, they are below the confidence level shown in black dashed curve in Fig-6(d). We repeat the analysis for cosmic ray modulation potential time series for the same temporal range. Regular activity phase for the normalized cosmic ray modulation potential is denoted by the solid red curve in Fig-7(a). The corresponding power spectrum which is concentrated around 11 year time period is plotted in Fig-7(b). In the bottom panel we plot the time series (see Fig-7c) and the respective power spectrum (see Fig-7d) in blue for grand minimum phase. For the cosmic ray modulation potential power corresponding to 11-year period decreases drastically for grand minimum phase as compared to the regular phase. The confidence level (CL) provides a bound on the significant periods in the power spectrum. In the long-term 6000 year simulation we find total four grand minimum phases. Spectral analysis was done independently on each epochs and we find consistent behaviour for all the cases.

We also perform spectral analysis on the 1000 year reconstructed OSF time series (Usoskin et al. 2021). The database contains OSF time series of the past 1000 years with an annual cadence. This reconstruction is based on the data of cosmogenic isotopes measured in terrestrial archives such as tree trunks or ice cores. We choose one of the Spörer minimum phase (which is a grand minimum) for our analysis which starts from 1390 and ends at 1550 (160 years). There are multiple other grand minimum episodes reported in the reconstructed data by Usoskin et al. (2016). Fig-8(a) shows the time series of reconstructed OSF for past $\sim$ 1000 years. We consider a period of 150 years from year 1100 to 1250 to be a regular solar activity phase which is plotted in red curve in Fig-8(b). Similarly we highlight the Spörer minimum phase in blue in Fig-8(d). The OSF time series that we analyzed for a regular activity phase and grand minimum phase is normalized to the maximum value of the 1000 year reconstructed OSF time series. We perform FFT analysis for both regular activity and the Spörer minimum phase. Fig-8(c) and (e) shows the power spectrum. The vertical dotted brown line denotes 11-year period for reference. The confidence level calculation is repeated for the reconstructed data and it is plotted in black dashed line in Fig-8 (c) and (e) for respective solar activity phases. The power corresponding to the dominant cycle period ($\sim$ 11 years) decreases during grand minimum phase in the reconstructed data as well. Earlier studies by Kane (2007); Zięba et al. (2006) also indicated the decrease in power corresponding to the 11-year solar cycle in their analysis. This demonstrates the qualitative consistency of spectral power distribution in the reconstructions and the solar dynamo modeled OSF.

4 CONCLUDING DISCUSSIONS

To summarize, we have simulated a 6000-year long solar activity series covering grand maxima, grand minima and regular activity phases utilizing a stochastically forced 2D solar dynamo model, and coronal magnetic field extrapolation based on the surface magnetic field configuration. We also calculate the OSF and the cosmic-ray modulation potential to understand the impact of solar activity on the state of the heliosphere.

Our results suggest that for the periods when there are no sunspot eruptions on the solar surface, not only the active region driven dynamics get suppressed, but also the polar flux decreases resulting in a decrease in the OSF and the cosmic ray modulation potential. Coronal magnetic field configuration during such periods indicates the presence of complex, closed magnetic loop-like structures near the polar latitudes ($\geq 70°$) which have weak magnetic field strength but, which may support the solar wind outflow.

Our study provides a theoretical basis for the past reconstructions of solar activity. As the Sun goes into a magnetically dormant phase, the net magnetic flux near the poles also decreases which leads to decrease in the overall OSF output. This in turn decreases the cosmic-ray modulation potential. Cosmic-ray flux and solar activity are negatively correlated. Reconstructions based on cosmogenic isotopes map the past solar activity cycle. Previous studies by (Usoskin et al. 2007; Wu et al. 2018) indicate the presence of grand maximum and minimum activity episodes in the reconstructed OSF time series. Solar dynamo model based calculation of the OSF and cosmic-ray modulation potential shows a significant decrease in these quantities for grand minimum phases. This bridges the gap between theory and reconstructions. Special states of the solar dynamo can push our star into a prolonged grand minimum episode leading to a reduction in the cosmic-ray modulation and open solar flux.

Solar coronal magnetic field dynamics plays an important role in determining heliospheric conditions including the origin of fast or slow solar wind, flares and coronal mass ejections. Flux transport processes shape the surface magnetic field, which generates the coronal magnetic field configuration. Magnetic flux is transported from the equatorial region towards the poles via the large-scale meridional circulation. Total solar eclipses illuminate these solar coronal configuration. Towards the end of the Maunder minimum (which is a grand

minimum phase), the solar eclipse paintings and predictions show a structure-less large-scale solar atmosphere Riley et al. (2015); Lockwood & Owens (2021); Hayakawa et al. (2021). However, we find complex low lying magnetic field structures in the solar corona during grand minimum phases in our extrapolated coronal magnetic field which are quite weak. Magnetic field strength is equally important for driving solar wind in the heliosphere. During low solar activity periods, the magnetic field strength reduces as the solar activity cycle weakens. Solar dynamo models can explain these different modes of solar activity fluctuation (Tripathi et al. 2021) and are used widely in solar cycle prediction studies (Bhowmik & Nandy 2018; Nandy 2021). The cosmogenic-isotope based reconstructions indicate presence of grand minima and maxima like phases that can be explained by solar dynamo theory.

Solar cycle has a periodicity of roughly 11 years. When solar activity is reduced during grand minimum phase, sunspot eruptions are suppressed on the surface. Our results show that for such phases, power stored in the 11-year solar cycle period is also reduced as observed in the computed heliospheric parameters like OSF and cosmic ray modulation potential and other frequencies manifest.

We conclude that the solar dynamo generated grand minimum, maximum and regular activity show complex magnetic loops which are distinct and leave an imprint in the heliospheric parameters like OSF and the cosmic ray modulation potential. Our study provides a theoretical basis for establishing causality between the solar dynamo mechanism and the long-term forcing of the state of the heliosphere.

ACKNOWLEDGEMENTS

The authors are thankful to Chitradeep Saha and Shaonwita Pal for helpful discussions and acknowledge discussions at the Workshop on "Solar and Stellar Dynamos: A New Era" sponsored by the International Space Science Institute, Bern, where the idea of this work was born. S.D. acknowledges funding from the DST-INSPIRE program of the Government of India. I.U. acknowledges partial support by the Academy of Finland (Project ESPERA No. 321882). The Center of Excellence in Space Sciences India (CESSI) is funded by IISER Kolkata, Ministry of Education, Government of India.

DATA AVAILABILITY

REFERENCES

Albert C., Ferriz-Mas A., Gaia F., Ulzega S., 2021, ApJ, 916, L9
Altschuler M. D., Newkirk G., 1969, Sol. Phys., 9, 131
Asvestari E., Usoskin I., 2016, Journal of Space Weather and Space Climate, 6, A15
Bharati Das S., Basak A., Nandy D., Vaidya B., 2019, ApJ, 877, 80
Bhowmik P., Nandy D., 2018, Nature Communications, 9, 5209
Brandenburg A., Spiegel E. A., 2008, Astronomische Nachrichten, 329, 351
Brehm N., et al., 2021, Nature Geoscience, 14, 10
Carbonell M., Oliver R., Ballester J. L., 1994, A&A, 290, 983
Charbonneau P., Dikpati M., 2000, ApJ, 543, 1027
Charbonneau P., Blais-Laurier G., St-Jean C., 2004, ApJ, 616, L183
Chatterjee P., Nandy D., Choudhuri A. R., 2004, A&A, 427, 1019
Choudhuri A. R., 1992, A&A, 253, 277
Choudhuri A. R., Karak B. B., 2012, Phys. Rev. Lett., 109, 171103
Dash S., Bhowmik P., Athira B. S., Ghosh N., Nandy D., 2020, ApJ, 890, 37
Hayakawa H., et al., 2020, ApJ, 897, L10
Hayakawa H., Lockwood M., Owens M. J., Sôma M., Besser B. P., van Driel-Gesztelyi L., 2021, Journal of Space Weather and Space Climate, 11, 1
Hazra S., Nandy D., 2019, MNRAS, 489, 4329
Hoyng P., Schmitt D., Teuben L. J. W., 1994, A&A, 289, 265
Isobe H., Ebihara Y., Kawamura A. D., Tamazawa H., Hayakawa H., 2019, ApJ, 887, 7
Kane R. P., 2007, Sol. Phys., 246, 487
Lockwood M., Owens M. J., 2014, Journal of Geophysical Research (Space Physics), 119, 5193
Lockwood M., Owens M., 2021, Astronomy and Geophysics, 62, 3.12
Lockwood M., Owens M. J., Barnard L. A., Scott C. J., Watt C. E., 2017, Journal of Space Weather and Space Climate, 7, A25
Moss D., Sokoloff D., Usoskin I., Tutubalin V., 2008, Sol. Phys., 250, 221
Nandy D., 2004, Sol. Phys., 224, 161
Nandy D., 2021, Sol. Phys., 296, 54
Nandy D., Choudhuri A. R., 2001, ApJ, 551, 576
Nandy D., Choudhuri A. R., 2002, Science, 296, 1671
Nandy D., Martens P. C. H., 2007, Advances in Space Research, 40, 891
Nandy D., Muñoz-Jaramillo A., Martens P. C. H., 2011, Nature, 471, 80
Nandy D., Bhowmik P., Yeates A. R., Panda S., Tarafder R., Dash S., 2018, ApJ, 853, 72
Nandy D., Martens P. C. H., Obridko V., Dash S., Georgieva K., 2021, Progress in Earth and Planetary Science, 8, 40
Pal S., Dash S., Nandy D., 2020, Geophys. Res. Lett., 47, e86372
Passos D., Nandy D., Hazra S., Lopes I., 2014, A&A, 563, A18
Potgieter M. S., 2013, Living Reviews in Solar Physics, 10, 3
Proctor M. R. E., 2007, MNRAS, 382, L39
Riley P., et al., 2015, ApJ, 802, 105
Schatten K. H., Wilcox J. M., Ness N. F., 1969, Sol. Phys., 6, 442
Schrijver C. J., De Rosa M. L., 2003, Sol. Phys., 212, 165
Schröder W., 1992, Journal of Geomagnetism and Geoelectricity, 44, 119
Silverman S. M., 1992, Reviews of Geophysics, 30, 333
Solanki S. K., Usoskin I. G., Kromer B., Schüssler M., Beer J., 2004, Nature, 431, 1084
Tripathi B., Nandy D., Banerjee S., 2021, MNRAS, 506, L50
Usoskin I. G., 2008, Living Reviews in Solar Physics, 5, 3
Usoskin I., 2017, Living Reviews in Solar Physics, 14, 3
Usoskin I., Mursula K., Solanki S. K., Schüssler M., Kovaltsov G. A., 2002, Journal of Geophysical Research (Space Physics), 107, 1374
Usoskin I., Solanki S. K., Schüssler M., Mursula K., Alanko K., 2003, Phys. Rev. Lett., 91, 211101
Usoskin I., Solanki, S. K. Kovaltsov, G. A. 2007, A&A, 471, 301
Usoskin I., et al., 2015, A&A, 581, A95
Usoskin I. G., Gallet Y., Lopes F., Kovaltsov G. A., Hulot G., 2016, A&A, 587, A150
Usoskin I., Solanki S. K., Krivova N., Hofer B., Kovaltsov G. A., Wacker L., Brehm N., Kromer B., 2021, VizieR Online Data Catalog, pp J/A+A/649/A141
Wu C. J., Usoskin, I.G. Krivova N., Kovaltsov G. A., Baroni M., Bard E., Solanki S. K., 2018, A&A, 615, A93
Zięba S., Masłowski J., Michalec A., Michałek G., Kułak A., 2006, ApJ, 653, 1517

This paper has been typeset from a TEX/LATEX file prepared by the author.

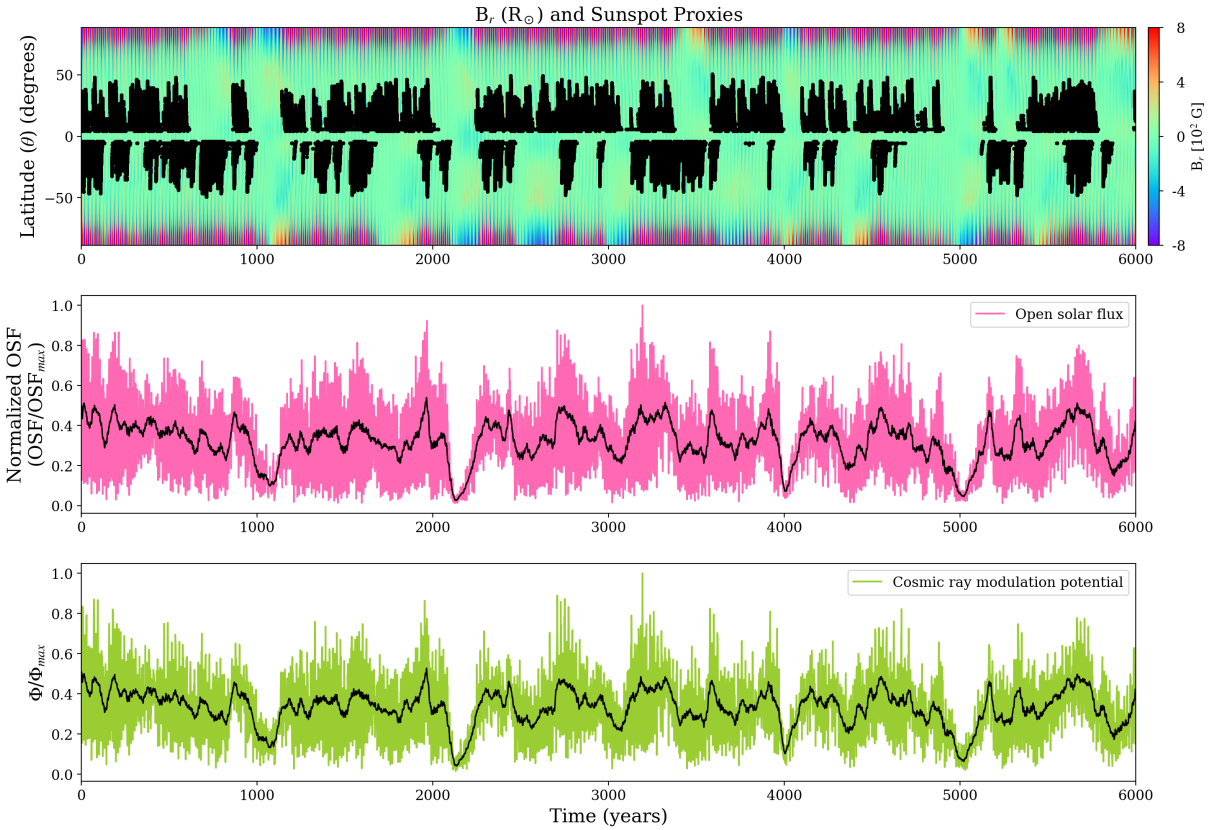

Figure 1. Long-term stochasticaly forced solar dynamo run for 6000 years. The top panel shows butterfly diagram of surface radial magnetic field (B_r). The sunspot eruption proxy latitudes are over-plotted in black. The middle panel denotes normalized open solar flux in magenta curve and a 22 year running average in solid black curve. In the lower panel we plot the normalized cosmic ray modulation potential in solid green color and the 22 year running average is plotted in solid black. During a grand minimum phase, there are no sunspot eruptions on the solar surface. Heliospheric modulation due to solar activity variation is indicated by the OSF and the cosmic ray modulation potential. In our simulation we find decrease in the OSF and cosmic ray modulation potential corresponding to grand minimum phases.

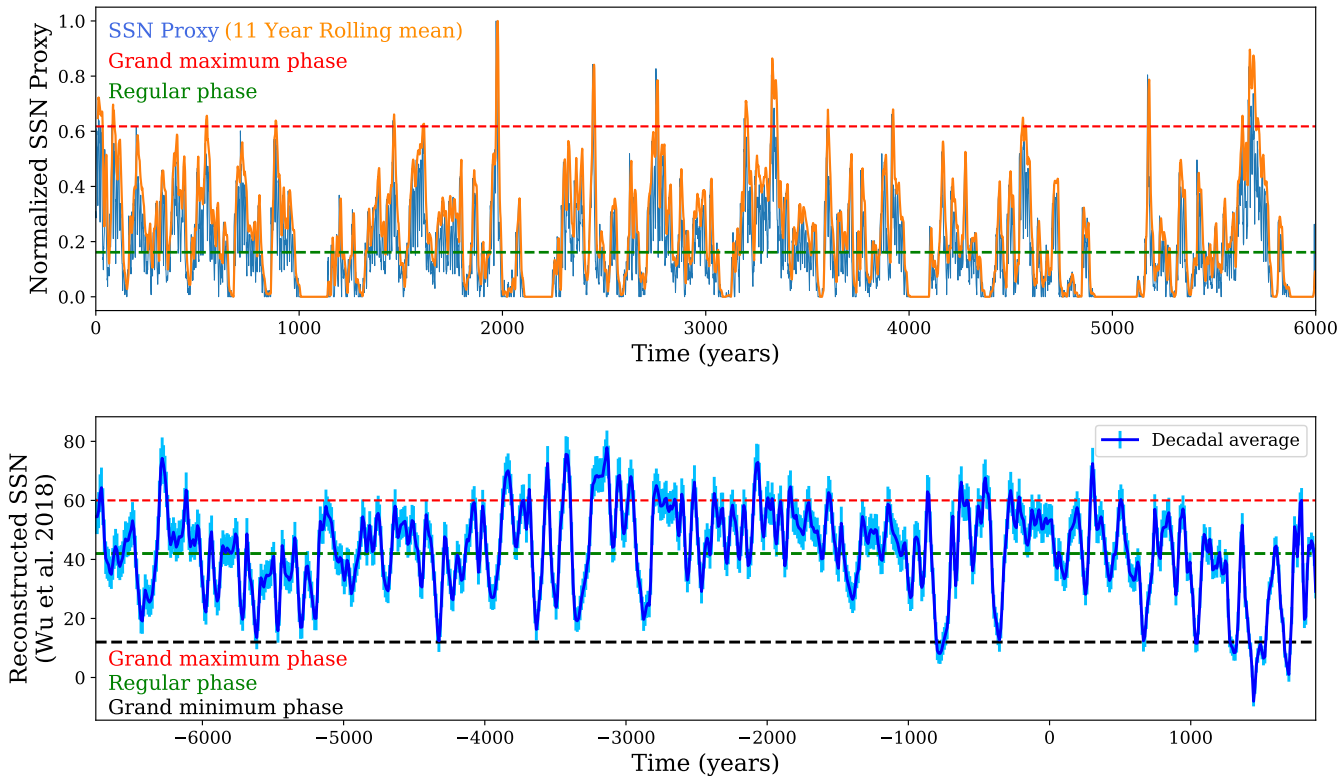

Figure 2. Sunspot number time series. Normalized time series of solar dynamo generated sunspot proxy for 6000 years is shown in blue in the top panel. Eleven year rolling mean of the SSN is plotted in orange to emphasize on the solar cycle behaviour. The mean sunspot number is plotted in green dashed curve. Episodes where the number of sunspots are greater than mean+3σ, are identified as grand maximum phase. Green dashed line here depicts the global mean of the SSN proxy distribution. Phases with no sunspot eruption proxies are the grand minimum phases in our simulation. Reconstructed decadal averaged SSN (Wu et al. 2018) is shown in blue in the bottom panel. Here the grand maximum phase is depicted by the dashed red curve. The green curve shows the main component (normal/moderate phase). The black dashed line denotes the grand minimum component of the reconstructed solar activity cycle. The presence of multiple grand maxima and grand minima phases is apparent in both reconstruction and the simulation.

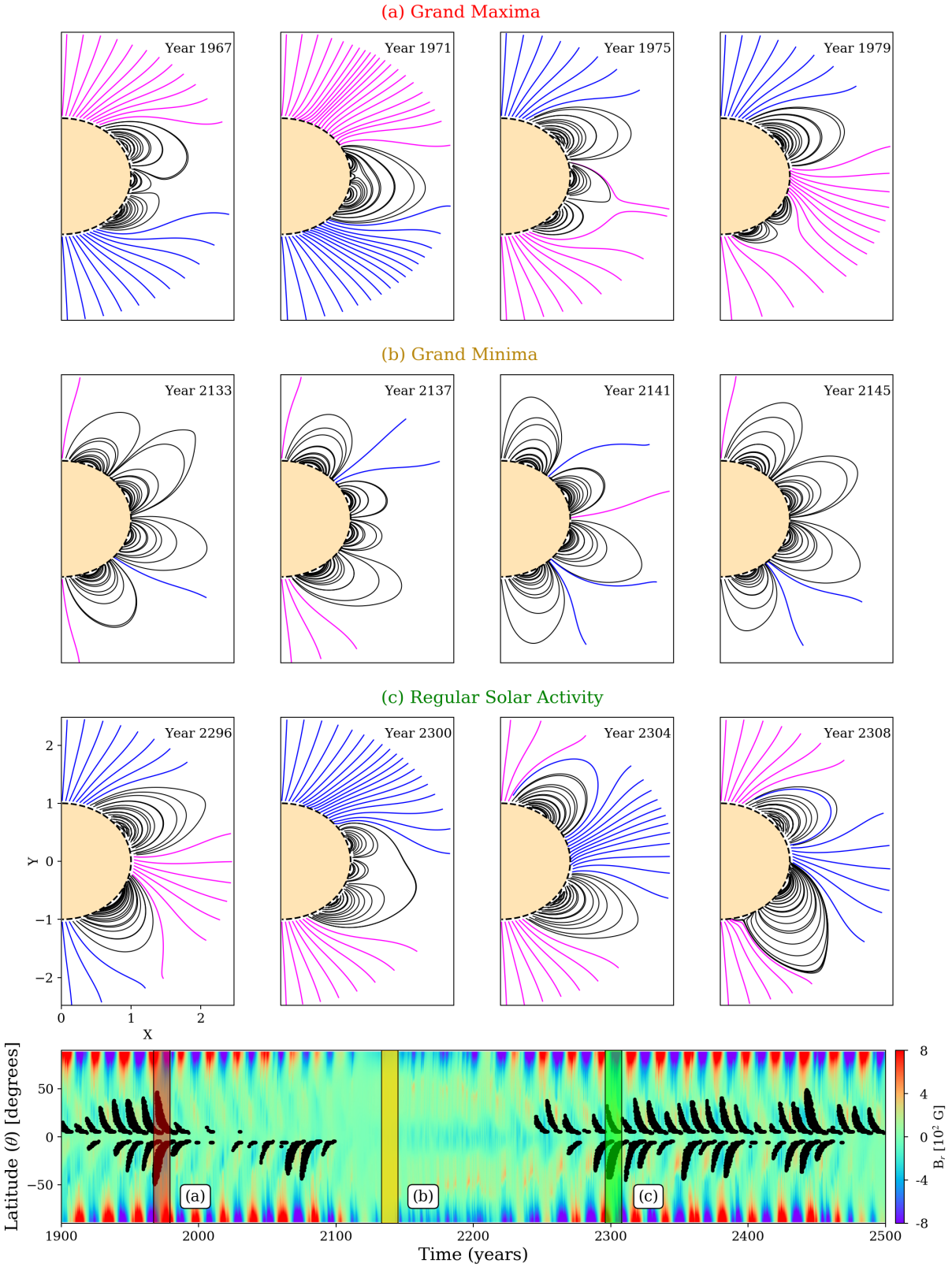

Figure 3. Evolution of solar coronal magnetic field configuration during grand maxima, grand minimum and a regular solar activity phase. In the bottom panel, surface radial magnetic field butterfly diagram and the sunspot eruption proxies in black are plotted. Shaded regions denote grand maxima (red), grand minima (yellow) and a regular solar activity (green) phase in the long-term solar dynamo simulation. They are labeled as (a), (b) and (c) respectively. For every segment we show the coronal magnetic field configuration starting from the cycle minimum (T0) in four increments. e.g. for the grand minimum episode distribution of coronal magnetic field for the year 2133, 2137, 2141, 2145 is shown where year 2133 and 2145 correspond to cycle minimum. Extrapolated coronal magnetic field lines are shown with open field lines denoted in blue (radially outward) and magenta (radially inward). Closed field lines are plotted in black. Complex coronal configuration consisting of closed magnetic field lines reaching close to polar regions are observed during grand minimum phase. Detailed analysis of the coronal magnetic field configuration for different epochs is provided in the text.

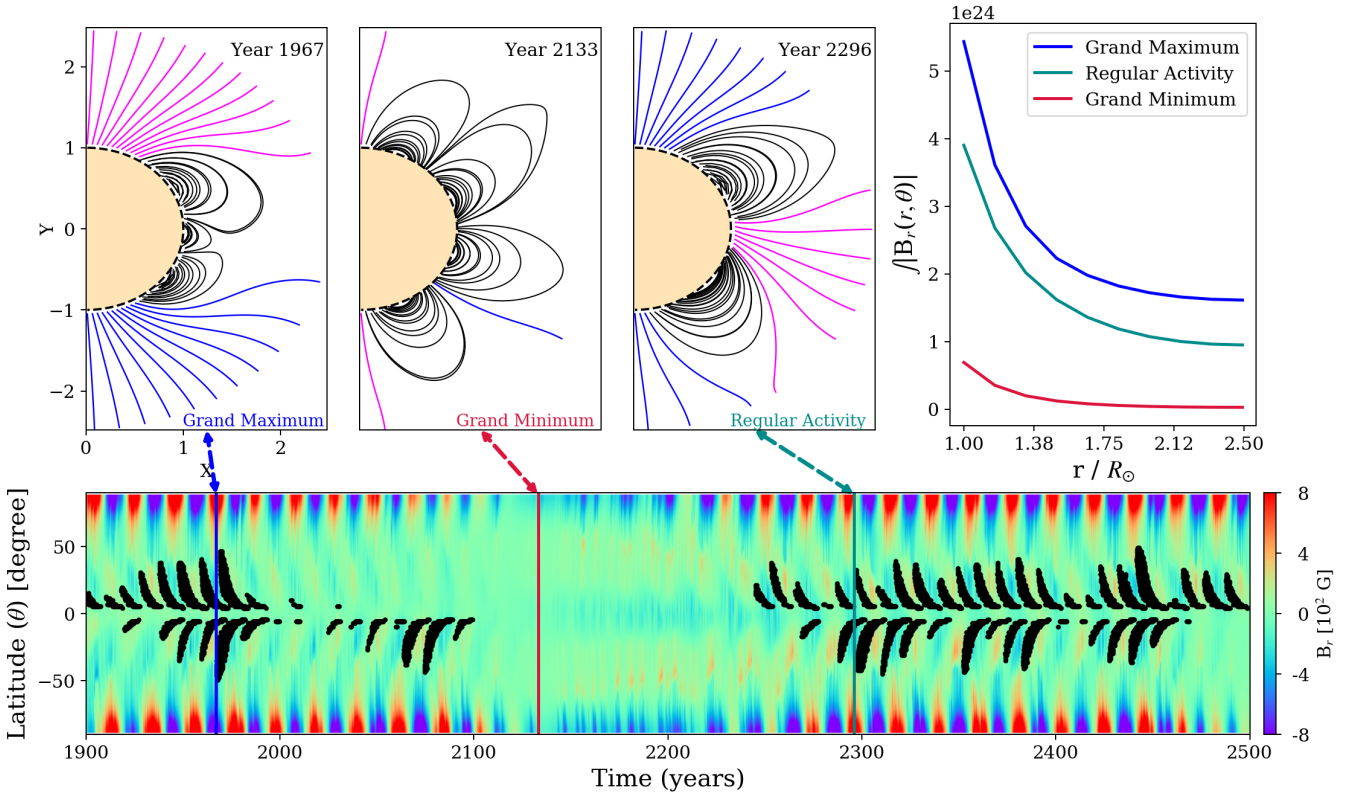

Figure 4. Reduction in magnetic field strength for different phases of solar activity. In our analysis year 1967 corresponds to an grand maxima phase. Similarly year 2133 and 2296 denote grand minimum phase and regular solar activity phase. The integrated radial magnetic flux across different radial heights is plotted in the top-right panel in blue (grand maxima), dark cyan (regular activity) and red (grand minimum). The decrease of over all flux from grand maxima to grand minima is observed in these three cases. At the source surface, the integrated quantity denotes the open solar flux. In the panel year 1967, year 2133, year 2296 the solar coronal magnetic field distribution is plotted corresponding to a grand maxima phase, grand minimum phase and regular activity phase respectively. In the butterfly diagram these regions are marked in solid lines for ease of understanding.

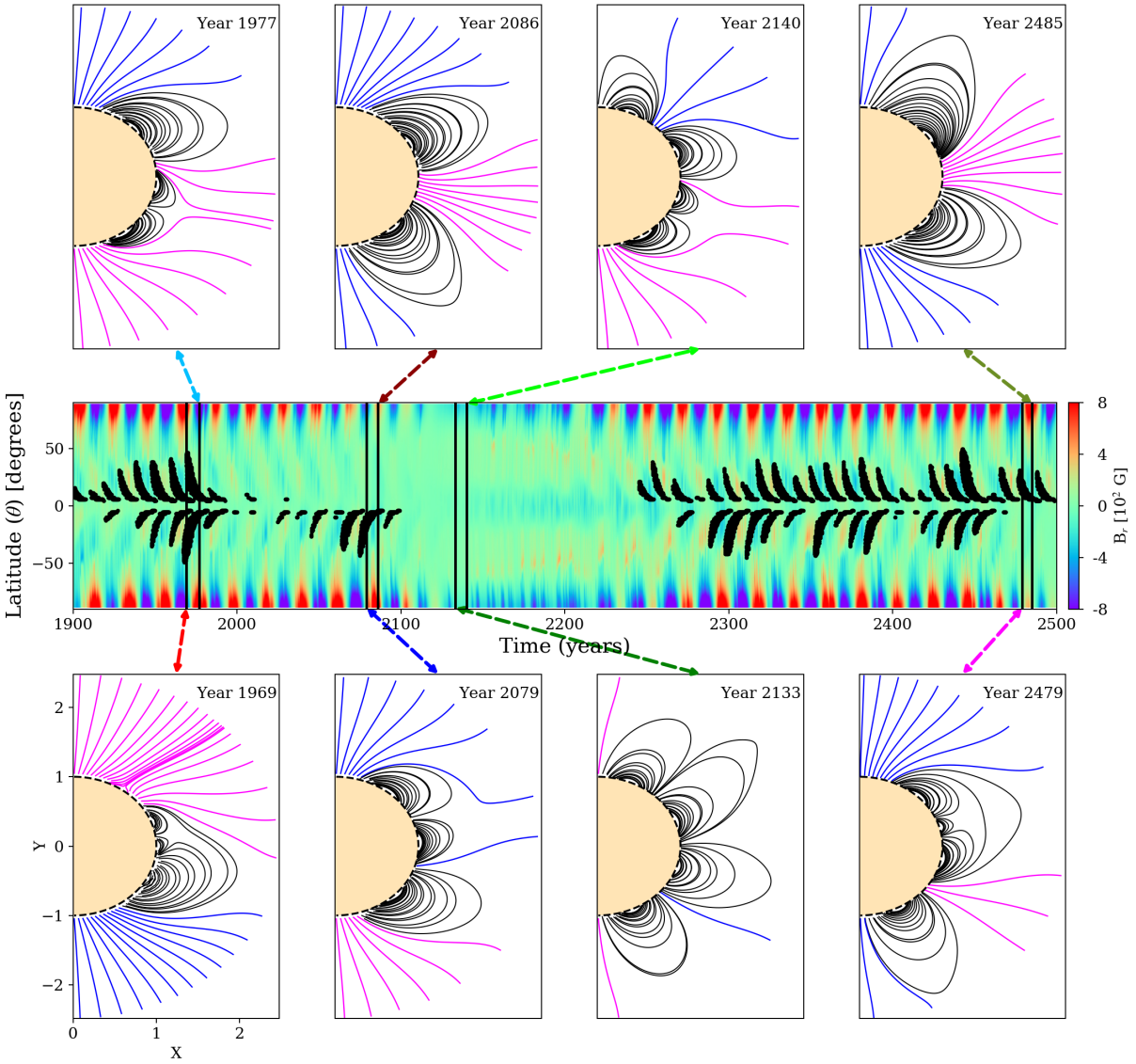

Figure 5. Solar coronal magnetic field configuration for different phases based on hemispheric sunspot eruptions. Central butterfly diagram shows a time frame spanning over 600 years from year 1900 to year 2500 with sunspot eruption proxies over-plotted in black. Global solar coronal magnetic field configuration is plotted for different cases. The black curve denotes closed magnetic fields and the magenta/blue show negative/positive open field lines. Year 1969 and 1977 demonstrates a period where the sunspot eruptions are observed till high latitudes in both the hemispheres in our simulation. For this case the coronal magnetic field distribution indicates presence of complex coronal loops closer to the equator. Year 2079 and 2086 denotes a period where eruptions are suppressed in the northern hemisphere. The resulting coronal magnetic field distribution shows a change in parity. Sunspot eruptions are absent for Year 2133 and 2140. For this case the magnetic field distribution is quite complex. We notice closed magnetic field lines even near polar regions. Sunspot eruptions are halted in the southern hemisphere for Year 2479 and 2485. We find a change in Sun's parity during this period.

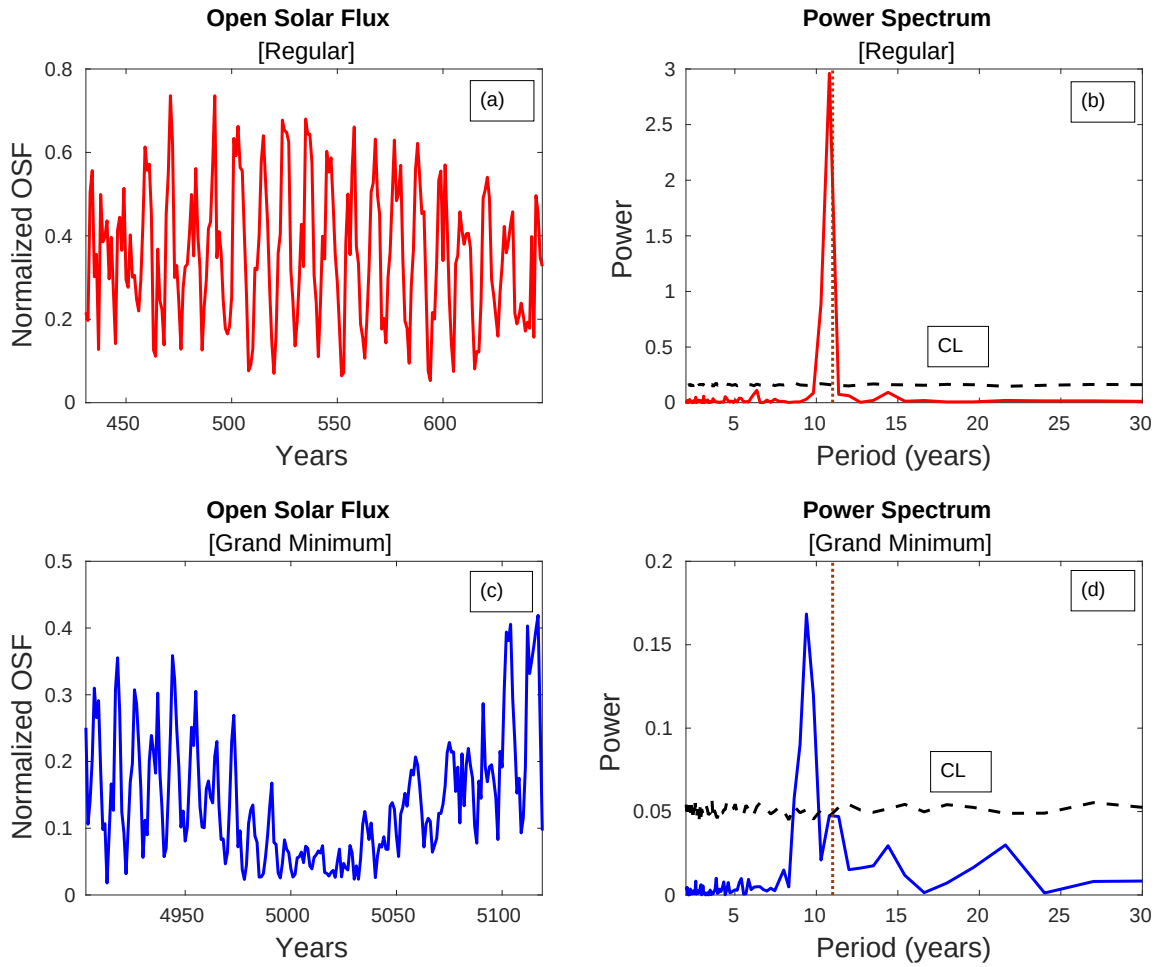

Figure 6. Spectral analysis on the simulated open solar flux time series. (a) The red curve indicates time series of normalized open solar flux for a regular activity phase (where there are finite sunspot proxies on the solar surface) from year 432 to 648. (b) The red curve shows the power spectrum of OSF for regular activity phase. FFT window size was chosen to be 1-year. The black dashed line denotes the upper 95th percentile of the FFT spectra for 1000 re-sampled open solar flux time series for the regular activity phase. (c) The blue curve shows the simulated open solar flux time series for one of the grand minimum episodes (year 4904 to 5120). (d) The power spectrum of open solar flux for the grand minimum phase. The black dashed line depicts the upper 95th percentile of the FFT spectra for 1000 re-sampled open solar flux time series for the grand minimum phase. Brown dotted line in the FFT spectra denotes the 11-year cycle period for reference. The spectral power corresponding to the dominant frequency decreases during the grand minimum phase compared to the regular activity phase.

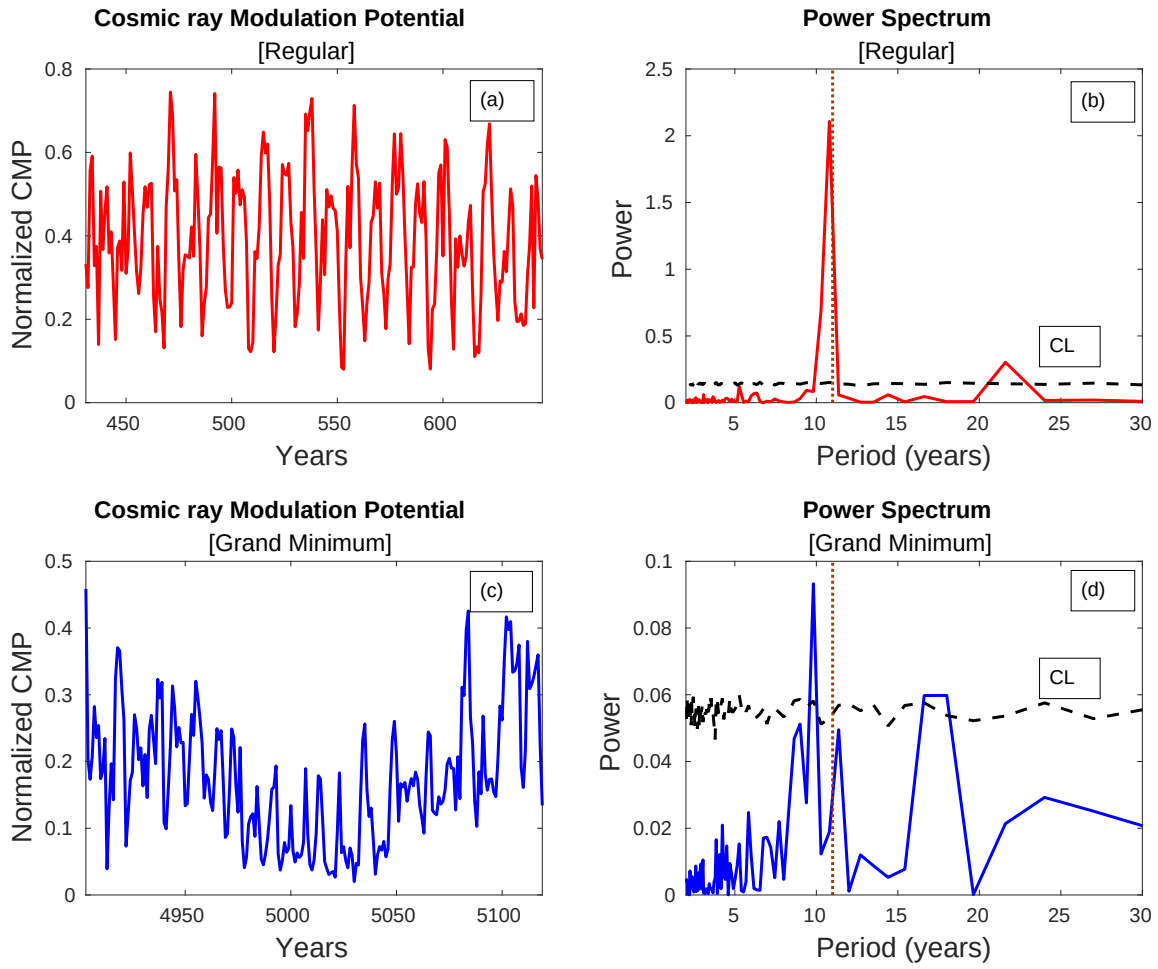

Figure 7. Spectral analysis on the simulated cosmic ray modulation potential time series. (a) The red curve indicates time series of normalized cosmic ray modulation potential for a regular activity phase (where there are finite sunspot proxies on the solar surface) from year 432 to 648. (b) The red curve shows the power spectrum of the time series. FFT window size was chosen to be 1-year. The black dashed curve denotes the upper 95th percentile of the FFT spectra of 1000 re-sampled cosmic ray modulation potential for the regular activity phase. This indicates the confidence level (CL). (c) The blue curve denotes the simulated modulation potential time series for one of the grand minimum episodes (year 4904 to 5120). (d) The power spectrum of the cosmic ray modulation potential for the grand minimum phase. The confidence level is plotted in black dashed line for this phase as well. Eleven year periodicity is shown with brown dotted curve on the FFT spectra. The power stored against the dominant frequency decreases during the grand minimum phases as compared to the regular phases.

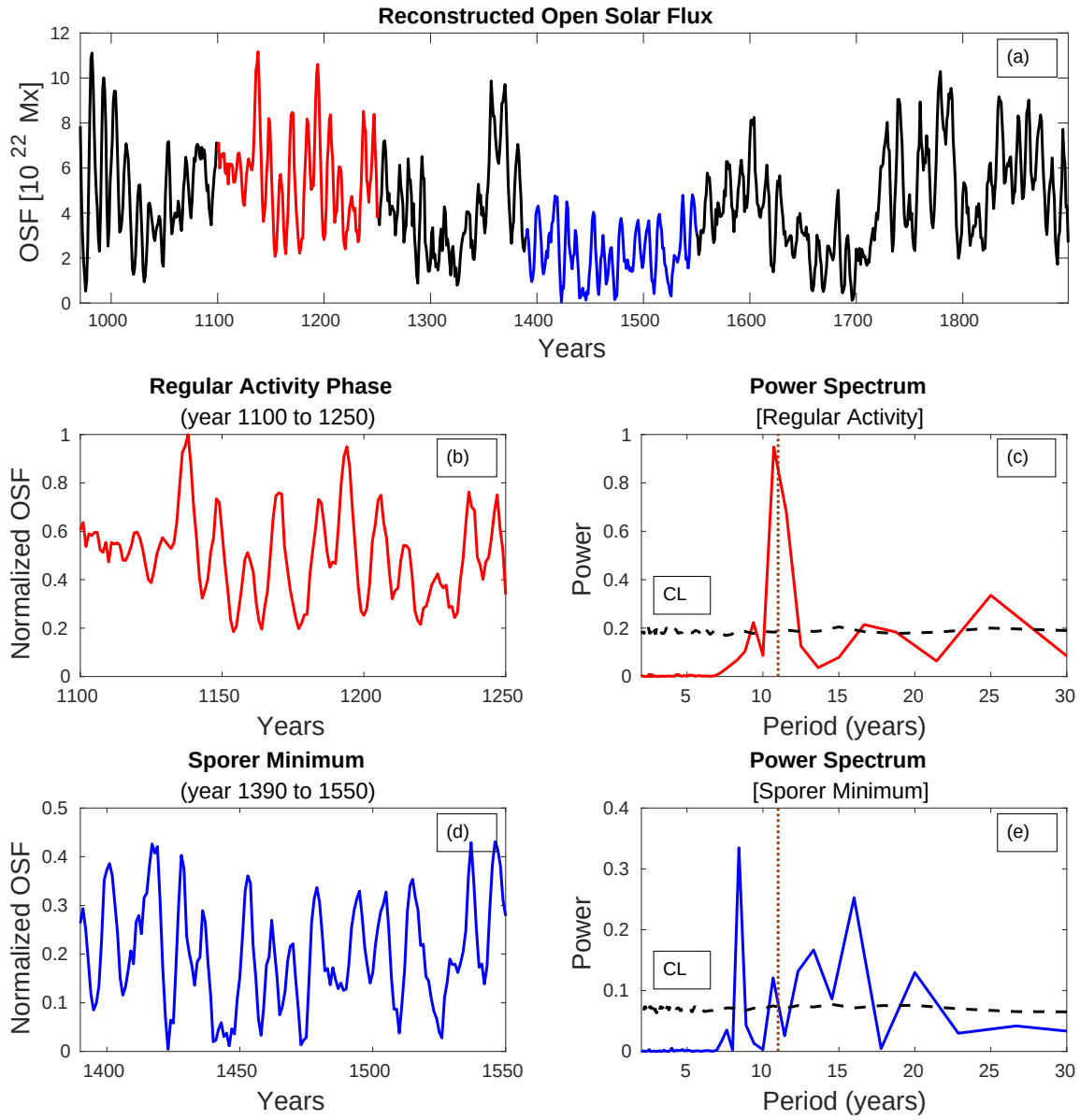

Figure 8. Fourier analysis of the reconstructed open solar flux. Reconstructed OSF data is obtained from Usoskin et al. (2021). (a) The time series of the open solar flux from 971 to 1899 is shown in solid black curve with the red colored region showing the regular activity phase (from year 1100 to 1250) and blue colored region – spanning from 1390 to 1550 – the Spörer minimum (one of the grand minimum episodes). (b) Normalized OSF for regular activity phase is shown in solid red curve. (c) The power spectrum of the regular activity phase is denoted by solid red curve. Here the brown dotted line denotes 11-year periodicity. (d) Normalized OSF for Spörer minimum phase is plotted in solid blue curve. Fourier power spectrum corresponding to the Spörer minimum phase is shown in panel (e). The solid black curve in panel (c) and (e) depicts the upper 95th percentile of the FFT spectra of 1000 re-sampled OSF data. This determines the confidence level (CL) of the dominant periods. The power stored in the dominant cycle period decreases significantly during grand minimum phase as compared to regular activity phase. We find similar trend in the simulated OSF as well.